AMERICAN SOCIETY FOR MICROBIOLOGY | Journal of Virology®

PATHOGENESIS AND IMMUNITY

# A MUC16 IgG Binding Activity Selects for a Restricted Subset of IgG Enriched for Certain Simian Immunodeficiency Virus Epitope Specificities

**Jeffrey R. Schneider,[a] Xiaoying Shen,[f,j] Chiara Orlandi,[k] Tinashe Nyanhete,[h,i] Sheetal Sawant,[f,j] Ann M. Carias,[b] Archer D. Smith IV,[n] Neil L. Kelleher,[l,m,n] Ronald S. Veazey,[o] George K. Lewis,[k] Georgia D. Tomaras,[g,h,i,j] Thomas J. Hope[b,c,d,e]**

[a]Department of Microbial Pathogens and Immunity, Rush University Medical Center, Chicago, Illinois, USA
[b]Department of Cell and Molecular Biology, Feinberg School of Medicine, Northwestern University, Chicago, Illinois, USA
[c]Department of Biomedical Engineering, Northwestern University, Evanston, Illinois, USA
[d]Chemistry of Life Processes Institute, Northwestern University, Evanston, Illinois, USA
[e]Department of Obstetrics and Gynecology, Northwestern University, Chicago, Illinois, USA
[f]Department of Medicine, Duke University, Durham, North Carolina, USA
[g]Department of Surgery, Duke University, Durham, North Carolina, USA
[h]Department of Immunology, Duke University, Durham, North Carolina, USA
[i]Department of Molecular Genetics and Microbiology, Duke University, Durham, North Carolina, USA
[j]Duke Human Vaccine Institute, Duke University, Durham, North Carolina, USA
[k]Division of Vaccine Research, Institute of Human Virology, University of Maryland School of Medicine, Baltimore, Maryland, USA
[l]Department of Chemistry, Northwestern University, Evanston, Illinois, USA
[m]Department of Molecular Biosciences, Northwestern University, Evanston, Illinois, USA
[n]Proteomic Center of Excellence, Northwestern University, Evanston, Illinois, USA
[o]Tulane National Primate Research Center, Tulane University School of Medicine, Covington, Louisiana, USA

**ABSTRACT** We have recently shown that MUC16, a component of the glycocalyx of some mucosal barriers, has elevated binding to the G0 glycoform of the Fc portion of IgG. Therefore, IgG from patients chronically infected with human immunodeficiency virus (HIV), who typically exhibit increased amounts of G0 glycoforms, showed increased MUC16 binding compared to uninfected controls. Using the rhesus macaque simian immunodeficiency virus SIVmac251 model, we can compare plasma antibodies before and after chronic infection. We find increased binding of IgG to MUC16 after chronic SIV infection. Antibodies isolated for tight association with MUC16 (MUC16-eluted antibodies) show reduced FcγR engagement and antibody-dependent cellular cytotoxicity (ADCC) activity. The glycosylation profile of these IgGs was consistent with a decrease in FcγR engagement and subsequent ADCC effector function, as they contain a decrease in afucosylated bisecting glycoforms that preferentially bind FcγRs. Testing of the SIV antigen specificity of IgG from SIV-infected macaques revealed that the MUC16-eluted antibodies were enriched for certain specific epitopes, including regions of gp41 and gp120. This enrichment of specific antigen responses for fucosylated bisecting glycoforms and the subsequent association with MUC16 suggests that the immune response has the potential to direct specific epitope responses to localize to the glycocalyx through interaction with this specific mucin.

**IMPORTANCE** Understanding how antibodies are distributed in the mucosal environment is valuable for developing a vaccine to block HIV infection. Here, we study an IgG binding activity in MUC16, potentially representing a new IgG effector function that would concentrate certain antibodies within the glycocalyx to trap pathogens before they can reach the underlying columnar epithelial barriers. These stud-

**Citation** Schneider JR, Shen X, Orlandi C, Nyanhete T, Sawant S, Carias AM, Smith AD, IV, Kelleher NL, Veazey RS, Lewis GK, Tomaras GD, Hope TJ. 2020. A MUC16 IgG binding activity selects for a restricted subset of IgG enriched for certain simian immunodeficiency virus epitope specificities. J Virol 94:e01246-19. https://doi.org/10.1128/JVI.01246-19.

**Editor** Guido Silvestri, Emory University



Address correspondence to Thomas J. Hope, thope@northwestern.edu.

**Received** 29 July 2019
**Accepted** 9 November 2019
**Accepted manuscript posted online** 27 November 2019
**Published** 14 February 2020

ies reveal that rhesus macaque IgG responses during chronic SIV infection generate increased antibodies that bind MUC16, and interestingly, these MUC16-tethered antibodies are enriched for binding to certain antigens. Therefore, it may be possible to direct HIV vaccine-generated responses to associate with MUC16 and enhance the antibody's ability to mediate immune exclusion by trapping virions within the glycocalyx and preventing the virus from reaching immune target cells within the mucosa. This concept will ultimately have to be tested in the rhesus macaque model, which is shown here to have MUC16-targeted antigen responses.

**KEYWORDS** antibodies, SIV infection, mucosal immunology

Recent human immunodeficiency virus (HIV)-related vaccine trials in humans and macaques show partial protection associated with antibodies (Abs) that do not show broadly neutralizing activity (1–3). Therefore, there is a greater interest in the potential effector function of these antibodies and the potential mechanism of protection. Recent effort has been accelerated toward understanding how nonneutralizing antibody activity could block HIV infection at mucosal surfaces (4).

Mucosal surfaces are the first barrier to pathogens in the female reproductive tract (FRT) and are protected by two distinct layers of mucins. The most superficial layer is composed of secreted gel-forming mucins, which constitutes mucus. Within the FRT, the gel-forming mucins include MUC5AC and MUC5B, which are secreted by goblet cells residing in the columnar epithelium of the endocervix. Between the columnar epithelial cells and the mucus is a covering of glycoproteins and glycolipids known as the glycocalyx. This layer contains the second layer of mucins, the cell-associated mucins. In the FRT, the cell-associated mucins present are MUC16 and MUC1 (5). Although these cell-associated mucins are shed into mucus, they are predominantly expressed on the epithelial surface to fortify the glycocalyx. Interestingly, in the case of MUC16, there is shedding from the uterodome during the receptive phase of the menstrual cycle (6). However, the overall mucin levels, both cell associated and gel forming, in cervical vaginal mucus are not altered throughout the menstrual cycle, but the glycosylation patterns on the mucins present are (5).

These protective layers also contain innate and adaptive immune proteins such as antibodies. In our previous studies, we demonstrated that some of these antibodies can tightly associate with FRT mucus (7). Other publications suggest that antibodies can work with mucus to inhibit pathogen movement by trapping in protective mucus layers (8, 9). Recently, we reported that the cell-associated mucin MUC16 contains an IgG binding function with preferential binding to IgG with a G0 glycoform (10), which is Fc mediated and of high affinity. MUC16 is a large cell-associated mucin, extending ~500 nm into the lumen and strategically located at the glycocalyx of the epithelium in mucosal surfaces such as the upper FRT and the lung (5, 11). This interaction would fortify the glycocalyx with antibodies that could facilitate pathogen trapping. We have found evidence that endogenous IgG colocalizes with MUC16 present on the surface of the endocervix, showing that this interaction is feasible *in vivo* (10). Having MUC16 and IgG localized to the endocervical epithelium could play a protective role; it has been shown that the entire FRT, from labia to ovaries, is a potential site of acquisition (12, 13).

The idea of antibodies trapping antigens in the mucosal lumen is not a novel concept and was originally described in 1975 using IgA (14). This process, known as immune exclusion, has been extended to the HIV field, whereby anti-HIV dimeric IgAs (dIgAs) can trap simian-human immunodeficiency virus (SHIV) in the mucosal layer, thus blocking infection (15, 16). Although systemic anti-HIV IgG has been shown to contribute synergistically to mucosal anti-HIV dIgA protection from SHIV infection (17), the potential for mucosal anti-HIV IgG to perform immune exclusion is just beginning to be shown. In a recent study, intrarectally applied anti-HIV IgG1 was shown to protect 5/6 rhesus macaques from intrarectal challenge (18). Although this study showed the feasibility of IgG to protect at the mucosal surface, an understanding of how to target IgG to the mucosa from a vaccine or passive infusion has yet to be elucidated.

IgG is glycosylated at asparagine 297 on the Fc portion of the antibody. Glycan branches extend corresponding to their galactose content, with G0 bearing no galactose, G1 having one galactose, and G2 having two galactose branches. These glycoforms can also contain fucose and have bisecting GlcNAc residues and terminal sialic acid moieties. During a state of inflammation, such as chronic HIV infection, these antibodies are modified toward a G0 state, meaning that they are galactose deficient (19). It is the enrichment of these antibodies to the G0 state during HIV infection that leads to the observed higher affinity for MUC16 (10). This tuning of glycoforms can influence the effector function of these antibodies (20). Therapeutic antibodies that are engineered to be afucosylated have the greatest potency for lymphoma treatment (21). HIV antibodies engineered with afucosylated and bisecting glycoforms have the highest binding to FcγRIIIa and have elevated antibody-dependent cellular cytotoxicity (ADCC) compared to other antibody glycoforms (22–24).

The potential importance of the Fc portion of HIV-specific antibodies and the effect of glycoform and IgG subclass on anti-HIV function is an area of robust debate (25). Reports focused on influenza and anthrax vaccines have shown a dependence of *in vivo* neutralization on Fc function (26–28). These results have been extended to work with HIV, demonstrating that Fc-engineered antibodies can exhibit increased neutralization, highlighting the dependence on Fc for blocking infection (29–31). However, the controversy continues relating to an HIV vaccine, as a pair of recent reports suggest that the Fc effector function, ADCC, is dispensable for blocking infection in the rhesus macaque SHIV challenge model (32, 33). It is likely that different antibodies and infection models emphasize different antibody functions to mediate protection. For example, it is a possibility that less-potent antibodies, such as b12, may require additional Fc effector functions to provide protection (34). Therefore, it is critical that the field better understand the protective mechanism of known antibody effector functions and seek to identify new potential effector functions to increase the potential efficacy of HIV vaccines in development.

Here, we show that IgG isolated from the plasma of simian immunodeficiency virus SIVmac251-infected rhesus macaques has increased binding to MUC16, relative to IgG from the same animals before infection. Isolation of the antibodies that bind most tightly to MUC16 revealed that these MUC16-eluted IgGs contain a distinct glycosylation profile, which skews them away from FcγR binding and ADCC effector function and toward increased MUC16 binding. Interestingly, these MUC16-eluted antibodies are enriched for certain SIV antigen specificities. The findings from this study suggest a novel effector function for some SIV-elicited antibodies, which are targeted to the glycocalyx through interaction with Fc receptors in MUC16. This would place such antibodies within overlying mucosal surfaces, imparting the potential to trap the virus before it could reach resident target cells and thus block infection by immune exclusion.

## RESULTS

**MUC16-eluted IgGs have elevated binding to MUC16 and a distinct glycosylation profile.** We recently reported an IgG binding activity in MUC16 that preferentially associates with glycoforms of IgG that are increased during chronic HIV infection (10). In order to assess whether this occurs in the rhesus macaque model, we obtained plasma from 6 rhesus macaques before and 150 days after SIVmac251 challenge. This is well beyond the 21- to 40-day acute-to-chronic SIV infection transition phase, and therefore, they were chronically infected (35). We first wanted to confirm that the MUC16 tissue distributions are similar between rhesus macaques and humans. Similar to our findings from previous work in the human endocervix, we found robust expression of MUC16 on the columnar epithelial surface of the rhesus macaque endocervix (Fig. 1A, MUC16 in red, E-cadherin in green, and nuclei in blue). IgG isolated from rhesus macaques that were chronically SIV infected had significantly elevated binding ($P$ value of $<0.05$ by a sign test) to MUC16 compared to IgG from the same macaques prior to infection, as shown by a MUC16 enzyme-linked immunosorbent

A.

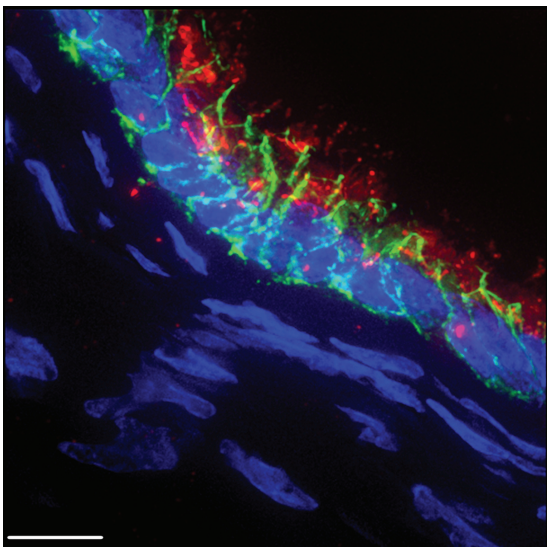

C.

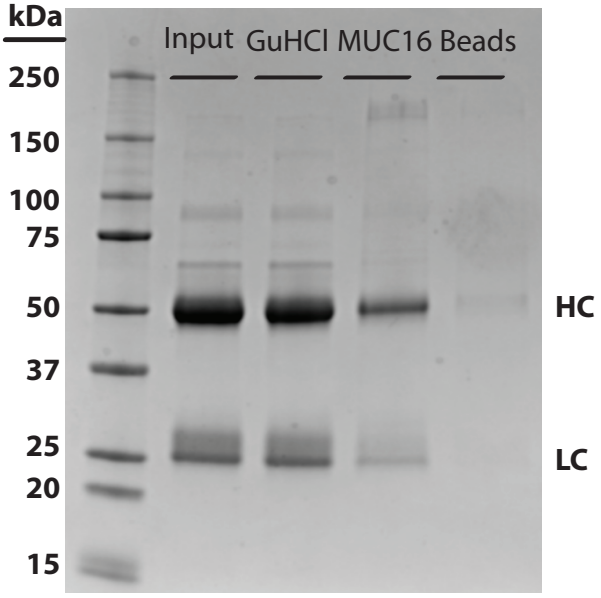


| Input IgG for capture | MUC16-eluted IgG yield | %MUC16 binding IgG |
|---|---|---|
| 500ug | 25.5ug | 5.1% |

B.

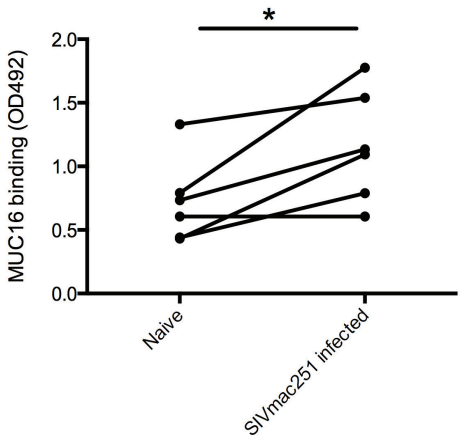


D.

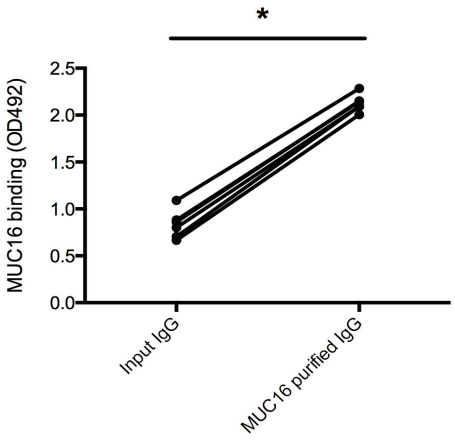


E.

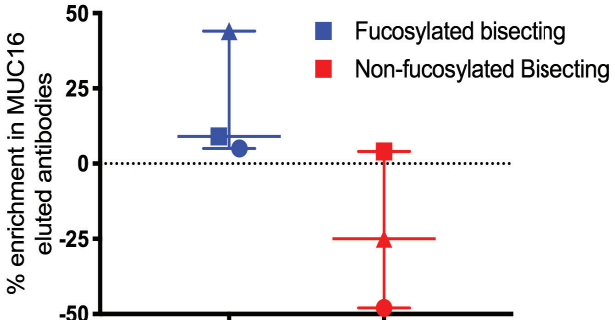


**FIG 1** Isolation and characterization of MUC16-eluted IgG from SIV-infected rhesus macaques. (A) Fluorescence deconvolution image (magnification, ×100) of MUC16 expression in rhesus macaque endocervical epithelium. Red, MUC16; green, E-cadherin; blue, nuclei. Bar, 10 $\mu$m. (B) MUC16 ELISA binding for plasma IgG before and after SIV infection ($n = 6$ rhesus macaques). (C) Isolation of the MUC16-eluted IgG using GuHCl, as shown by Coomassie staining on an SDS-PAGE gel. HC denotes the heavy chain, and LC denotes the light chain. The table shows the percent yield of MUC16-eluted IgG. (D) MUC16 ELISA binding for plasma IgG before and after MUC16 purification ($n = 6$ rhesus macaques). (E) Proteomic analysis of glycoforms enriched in MUC16-eluted IgG compared to GuHCl-treated input controls ($n = 3$ rhesus macaques). Median values are displayed as center bars, with error bars showing the ranges. Each symbol (triangle, square, and circle) represents an individual monkey. *, $P$ value of $<0.05$ by a sign test.

assay (ELISA) (Fig. 1B). With the exception of one rhesus macaque, all the protein G-purified IgG showed elevated binding to MUC16 following SIV infection. Therefore, we were able to recapitulate the increase in MUC16 binding following infection that we see in human subjects in the rhesus macaque model.

Next, we wanted to isolate and characterize the antibody subset that is most responsible for this elevated binding to MUC16. Utilizing an established tosyl-activated magnetic bead-based purification method, we isolated MUC16-eluted IgG from each animal. This high-affinity Fc-mediated interaction is reminiscent of C1q binding to IgG, where there is a small subset of antibodies that bind very tightly and are not dissociated under standard dissociation conditions, such as 3 M NaCl, 5 M urea, or beta-mercaptoethanol (36). Under the conditions of this experiment, the bound IgG could be eluted only by denaturation with 6 M guanidine hydrochloride (GuHCl) followed by a refolding step where GuHCl is removed by buffer exchange into phosphate-buffered saline (PBS). Because the refolding process could potentially influence antibody activity, we included an important control where input IgG was denatured with GuHCl followed by buffer exchange back to PBS prior to being used in functional assays (10). In the presented Coomassie-stained gel (Fig. 1C), the 3 antibody populations, from 1 representative monkey used in this study, are shown through the process of purification: input IgG, GuHCl-treated input IgG, and MUC16-eluted IgG. As is evident from the Coomassie-stained gel, the purified MUC16-eluted IgG is a minority species and represents roughly 5% of the total input IgG that went into to the purification (calculated by dividing MUC16-eluted IgG that was yielded by the total input IgG that was incubated with the MUC16 beads) (Fig. 1C). In addition, the Coomassie-stained gel reveals that the isolation process of the MUC16-bound IgG does not lead to IgG degradation. Importantly, there is very little IgG remaining on the tosyl-activated beads after purification (Fig. 1C, last lane), showing that the detachment of IgG from MUC16 beads was efficient. Next, we wanted to confirm that enrichment for MUC16 binding IgG resulted in an enrichment of binding to MUC16. MUC16-eluted IgG indeed had elevated binding to MUC16 compared to input IgG for all 5 of the purified samples (Fig. 1D) ($P$ value of $<0.05$ by a sign test) and therefore was enriched for MUC16 binding.

Previously, we showed that MUC16-associated human IgG has a distinct glycosylation profile, an enrichment in fucosylated bisecting glycoforms, compared to input IgG (10). Therefore, we wanted to assess whether these MUC16-associated IgGs also have a distinct glycosylation pattern. We evaluated antibodies from 3 randomly chosen monkeys for proteomic glycosylation analysis and found an increase in fucosylated bisecting glycoforms (Fig. 1E, blue symbols) and a decrease in afucosylated bisecting glycoforms (red symbols) in MUC16-eluted IgG relative to input IgG, similar to what is observed in human studies (10). Thus, we can purify a MUC16-eluted IgG population with a distinct glycosylation profile from the plasma of SIV-infected rhesus macaques.

**MUC16-eluted IgG has reduced binding to Fc$\gamma$Rs and is deficient at performing ADCC.** MUC16-eluted IgG was next assessed for Fc-mediated effector functions. First, the binding of MUC16-eluted IgG from 3 SIV-infected rhesus macaques to rhesus macaque Fc$\gamma$RIIA, -IIB, and -IIIA (each of them being allele 1) was determined by an ELISA. As a control, GuHCl-treated input antibodies were also evaluated. To compare binding, the median area under the curve (AUC) was measured, a reliable method for evaluating antibody titrations (37, 38). MUC16-eluted IgG had decreased binding to all rhesus macaque Fc receptors compared to GuHCl-treated control antibodies (Fig. 2A to C), as expected based on the glycosylation profile of these MUC16-eluted IgGs. All the Fc$\gamma$Rs had similar reductions in the median AUC, with Fc$\gamma$IIIA having a 36.7% reduction, Fc$\gamma$IIB having a 41.7% reduction, and Fc$\gamma$RIIA having a 40.4% reduction. Therefore, although the MUC16-eluted antibodies have an enriched association with MUC16 (Fig. 1D), they have decreased Fc$\gamma$R binding compared to GuHCl-treated input antibodies.

We next measured the impact of this decrease in Fc$\gamma$R engagement by MUC16-eluted IgG on effector function activity. Since we observed an increase in fucose in MUC16-eluted IgG in both humans and monkeys, we next carried out an assay to measure ADCC, as it has been shown that ADCC activity is inversely correlated with the

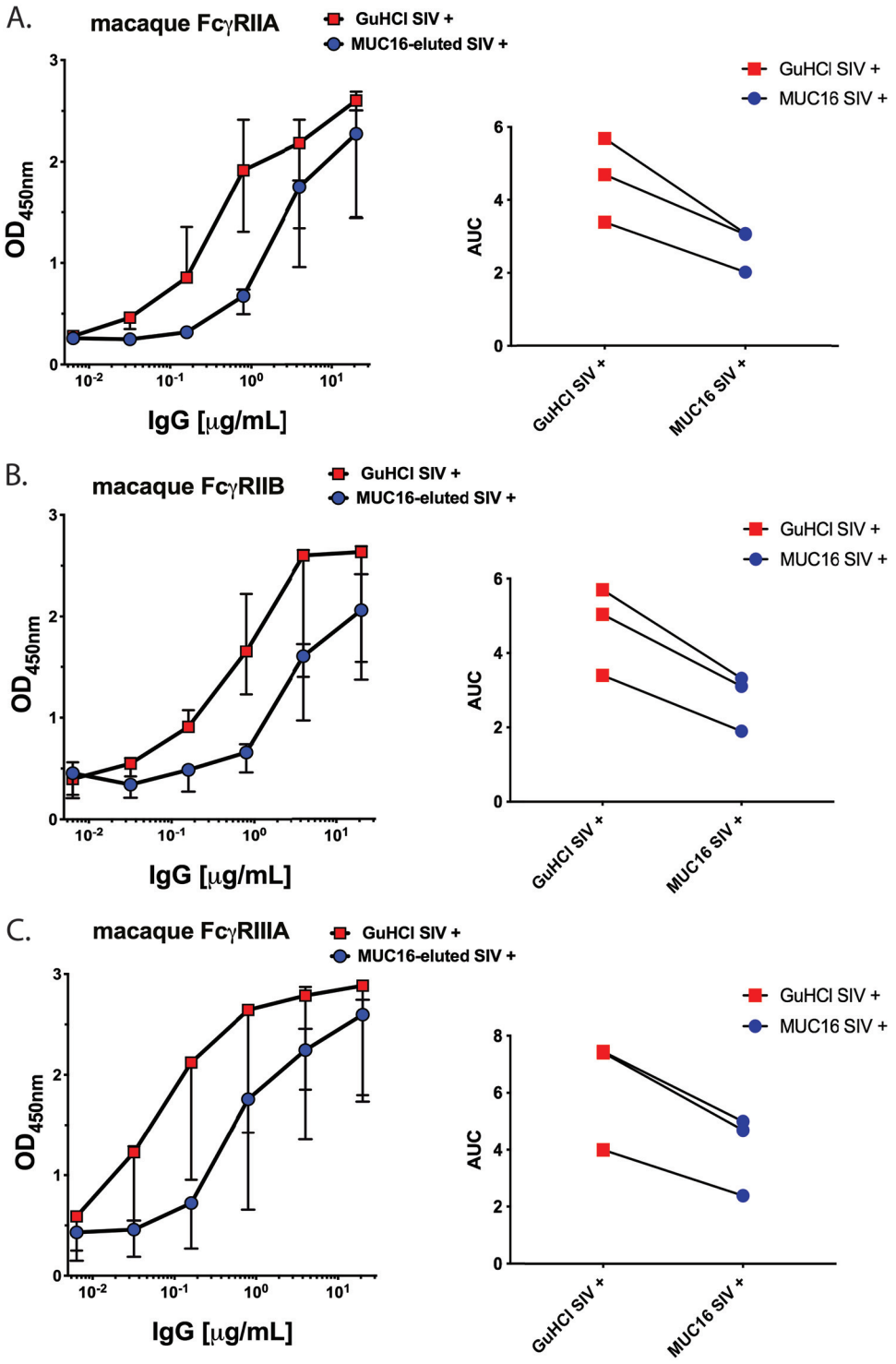


**FIG 2** FcγR ELISA binding of MUC16-eluted IgG. Binding to rhesus macaque low-affinity FcγRs (FcγRIIA, -IIB, and -IIIA) was determined for MUC16-eluted IgG compared to SIV-positive GuHCl-treated input IgG ($n = 3$ SIV$^+$ rhesus macaques). Median values are displayed as center bars, with error bars showing the ranges. The area under the curve (AUC) was measured for each graph.

presence of fucose (10). We did not investigate antibody-mediated cellular phagocytosis (ADCP) activity as this process occurs independently of fucose (39). To assess ADCC, we used a modified rapid fluorometric ADCC (RFADCC) assay, where CCR5-snap-tagged EGFP-CEM-NKr target cells are sensitized with SIV CM239 AT-2 inactivated virus

by spinoculation and incubated with antibodies along with peripheral blood mononuclear cells (PBMCs) as effector cells (40). Cellular cytotoxicity is determined by measuring the decrease in enhanced green fluorescent protein (EGFP) expression in CCR5-snap tag-expressing cells, i.e., cell lysis due to ADCC (40). Input IgG, GuHCl-treated input IgG, and MUC16-eluted IgG from 4 SIV-positive ($SIV^+$) and 3 SIV-negative ($SIV^-$) rhesus macaques were assessed for their ability to induce cytotoxicity in target cells. As a positive control, we utilized a rhesus macaque monoclonal antibody, 311.H (gp120 V3 loop), with known ADCC activity in this assay. As negative controls, we utilized a rhesus macaque monoclonal antibody, 6.10B (gp120 CD4 binding site [CD4bs] and CCR5 binding site [CCR5bs]) and a commercially available anti-respiratory syncytial virus antibody, Synagis. The gating strategy for measuring percent cytotoxicity is shown for the positive-control antibody 311.H (Fig. 3A) and for MUC16-eluted IgG (Fig. 3B). The ADCC potency of the tested IgGs was calculated by back-gating the number of the target cells losing the EGFP signal but retaining the CCR5-snap tag, compared to the total number of target cells (gate P3 in Fig. 3A and B). Whereas input IgG and GuHCl-treated input IgG showed efficient killing of target cells, MUC16-eluted IgG had a decrease in ADCC activity (Fig. 3C, blue symbols). Similar to the analysis of Fc$\gamma$R binding, the median AUC was measured to show differences in cytotoxicity. For all 4 matched GuHCl-treated and MUC16-eluted samples, the MUC16-eluted AUC was lower, and the median AUC was reduced by 66.8% (Fig. 3D). The low level of ADCC activity of these MUC16-eluted IgGs was most comparable with that of the negative-control monoclonal SIV IgG antibody 6.10B (Fig. 3D, purple symbol) and similar to that of the input from the animals before SIV infection (yellow and black symbols). Therefore, the MUC16-eluted antibodies are unable to perform the classical IgG effector functions of Fc$\gamma$R binding and ADCC activity, illustrating a distinct specialized effector function of MUC16 binding which would localize this population of antibodies to the glycocalyx.

**MUC16-eluted SIV IgG is enriched for gp41 whole-antigen binding plus gp41 and V2 linear peptide binding.** Next, we evaluated the antigen specificity of the MUC16-eluted antibodies to demonstrate that the SIV-specific antibodies generated during chronic SIV infection could associate with MUC16 and mediate immune exclusion by trapping in the glycocalyx. Therefore, we isolated MUC16-eluted IgGs from 14 SIVmac251-infected and 2 noninfected rhesus macaques and evaluated their SIV antigen binding using a panel of SIV antigens in an established and validated Luminex bead-based assay (41). The IgG from all the noninfected rhesus macaques revealed no SIV antigen binding (data not shown). Next, we probed antigen binding in the input IgG, GuHCl-treated input IgG, and MUC16-eluted IgG from 14 SIVmac251-infected rhesus macaques. Whereas the magnitudes of binding to gp120, gp130, and gp140 SIV Env antigens were comparable between input, GuHCl-treated input, and MUC16-eluted IgG (Fig. 4A to D), there was a significant increase in binding to gp41 for MUC16-eluted IgG (Fig. 4E) (raw $P$ value = 0.002; false discovery rate [FDR] $P$ value = 0.027). Binding to Gag proteins (p55 and p27) was slightly lower for the MUC16-eluted IgG than for the GuHCl-treated input albeit without statistically significant differences (Fig. 4F and G).

In order to investigate this increase in gp41 specificity further, we next measured linear antigen peptide binding to MUC16-eluted IgG from 8 SIVmac251-infected rhesus macaques to further map the antibody binding epitope. In addition, we included gp120 linear peptide epitopes to interrogate gp120 interactions beyond whole-antigen binding, as linear peptide binding does not always translate to what is observed using whole antigens. Purified antibodies were screened against overlapping peptides covering full-length SIVmac239 and SIVsmE660 Envs, including V2 (amino acids [aa] 163 to 183), V3 (aa 302 to 312), V3 (aa 320 to 343), V4 (aa 419 to 437), C5 (aa 501 to 524), gp41 immunodominant domain (gp41-ID) (aa 600 to 626), C-gp41-ID (aa 618 to 632), and Kennedy epitope (KE) (aa 711 to 734) regions. In the gp41 region, binding to the C-gp41-ID (aa 618 to 632) immunodominant epitope was found to be significantly higher in the MUC16-eluted IgG than in the GuHCl-treated input IgG (Fig. 5) (raw $P$ value = 0.008; FDR $P$ value = 0.039). There was also a statistically significant increase in binding to the V2 (aa 163 to 183) linear peptide (Fig. 5) (raw $P$ value = 0.008; FDR $P$

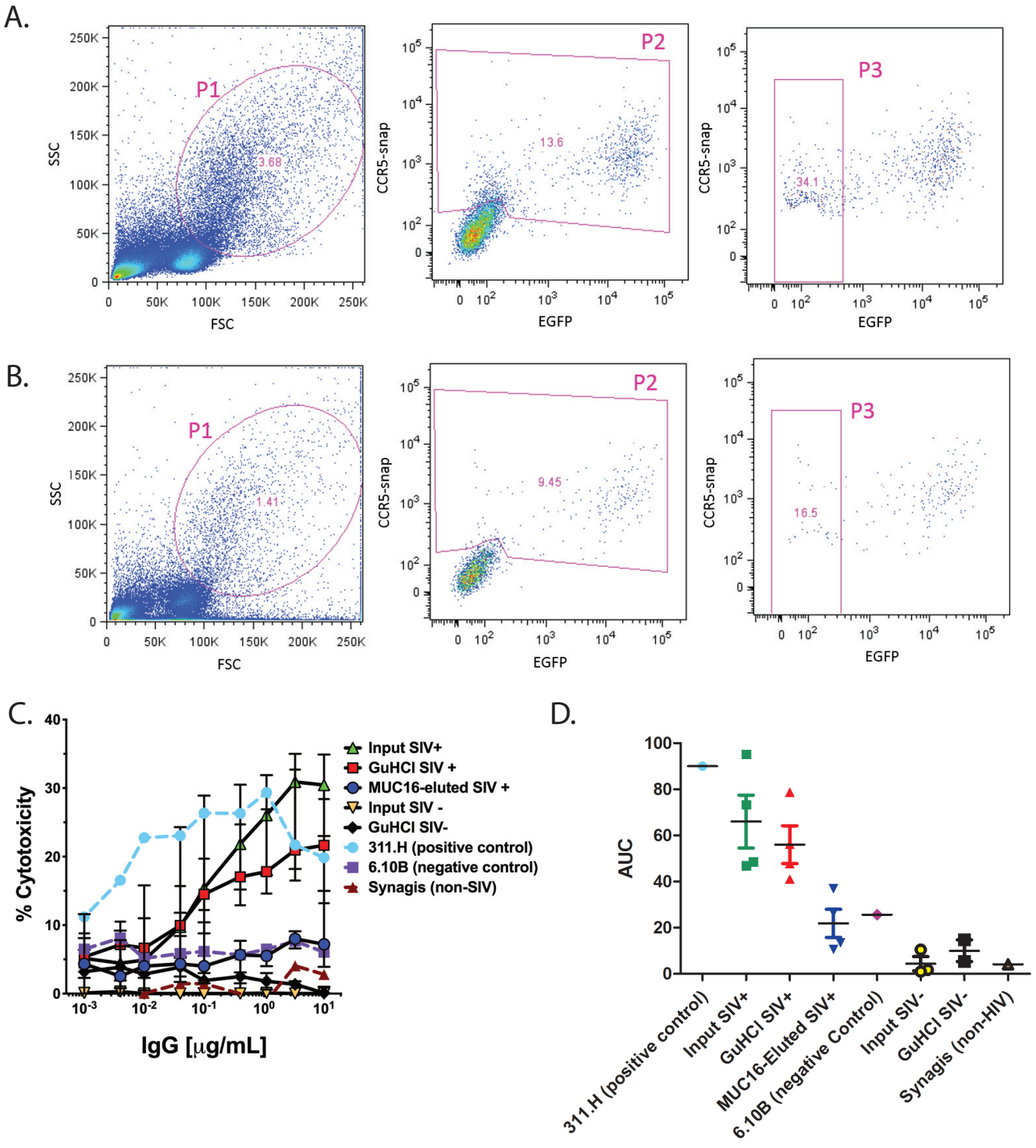


**FIG 3** ADCC activity of MUC16-eluted IgG. (A and B) Gating strategy for percent cytotoxicity in the positive-control antibody 311.H (A) and MUC16-eluted IgG (B). SSC, side scatter; FSC, forward scatter. (C) The ADCC activity of MUC16-eluted IgG was quantified by a modified RFADCC assay. As a reference, the input IgG and GuHCl-treated IgG from SIV-positive and -negative animals were used. In addition, a positive control, 311.H, and negative controls, 6.10B and Synagis, were used ($n = 4$ $SIV^+$ and 3 $SIV^-$ rhesus macaques). Median values are displayed as center bars, with error bars showing the ranges. (D) The area under the curve was calculated under each condition.

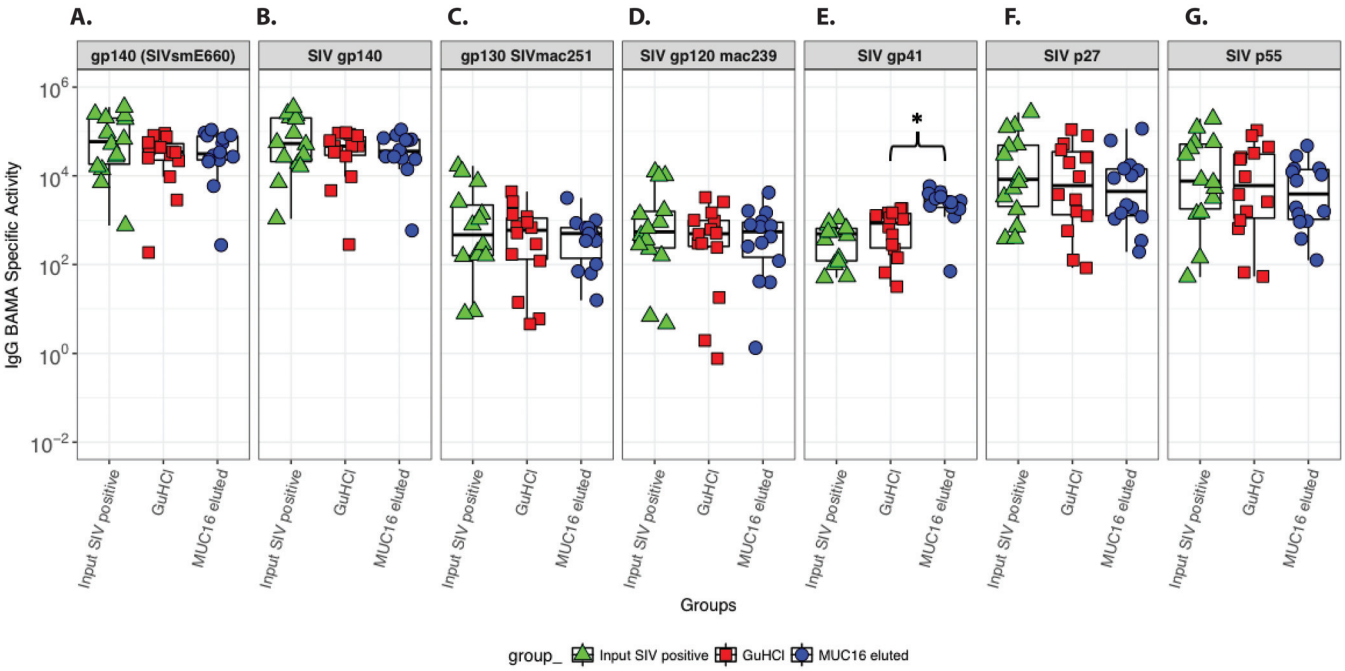


**FIG 4** Binding of MUC16-eluted IgG to SIV antigens. SIV antigen binding specificities of the different IgG fractions, input IgG, GuHCl-treated IgG, and MUC16-eluted IgG, are shown. Binding was assayed for gp140 SIVsmE660 (A), SIV gp140 (B), SIVmac251 gp130 (C), SIVmac239 gp120 (D), SIV gp41 (E), SIV p27 (F), and SIV p55 (G). IgG BAMA specific activity was calculated as the ratio of [blank and background-subtracted MFI (within the linear range of the BAMA) × dilution]/total IgG (micrograms per milliliter). Each point represents an individual macaque ($n = 14$ rhesus macaques). *, FDR-corrected $P$ value of $<0.05$ by a sign test.

value = 0.039). V3 (aa 320 to 343) epitope binding was elevated in the MUC16-associated IgG, without achieving statistical significance (Fig. 5) (raw $P$ value = 0.07; FDR $P$ value = 0.21). In contrast, V3 (aa 302 to 312), C5 (aa 501 to 524), and gp41 (aa 600 to 626) binding all trended lower in the MUC16-associated IgG, albeit insignificantly, than in the GuHCl-treated bulk IgG, and V4 binding (aa 419 to 437) and KE binding (aa 711 to 734) were similar between the fractions. Thus, subsets of MUC16-eluted antibodies are enriched for particular SIV specificities, as shown through native

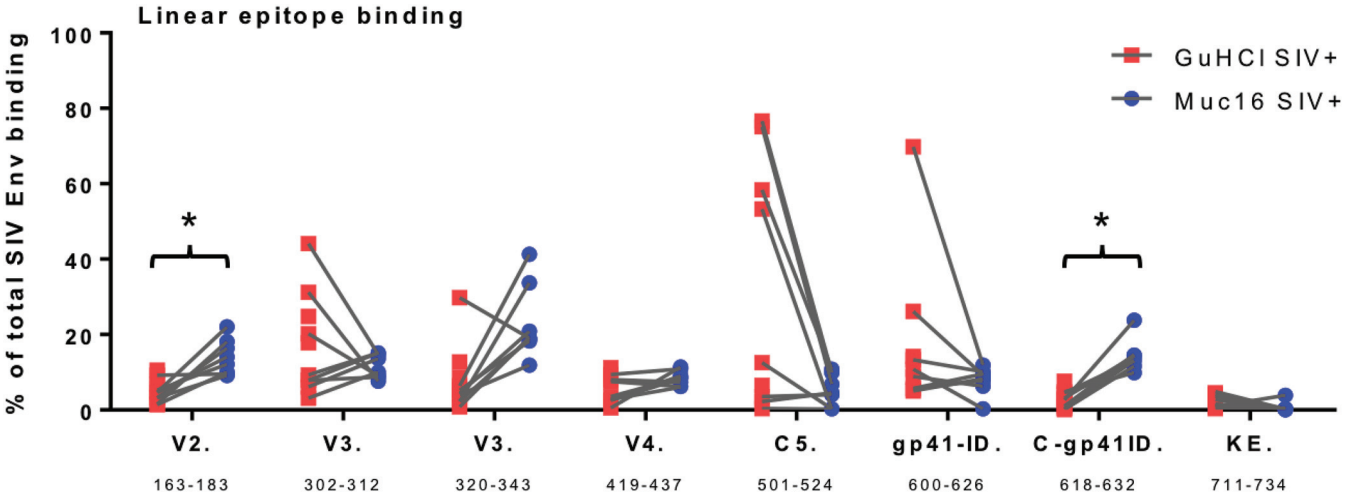


**FIG 5** Linear peptide binding to MUC16-eluted IgG. Linear epitope mapping of purified IgG (GuHCl control and MUC16 eluted) against overlapping peptides covering full-length SIVmac239 and SIVsmE550 Envs was performed. Linear epitope regions are indicated along the $x$ axis with amino acid position ranges (by SIVmac239 numbering). The percentage of total Env binding for each epitope is calculated as 100 × the magnitude of binding to each epitope/sum of the magnitude of binding to all epitopes ($n = 8$ rhesus macaques). *, FDR-corrected $P$ value of $<0.05$ by a sign test.

antigen and linear peptide binding. This reveals that during the immune response to a specific antigen, the resulting antibodies can be targeted to fortify the glycocalyx.

## DISCUSSION

In this study, we took advantage of the unique features of SIV infection in the rhesus macaque model to gain insights into how the resulting SIV-specific antibodies produced during chronic infection could interact with MUC16 through their Fc domain. Antibodies enriched for MUC16 association were characterized, and insights into the potential mucin binding effector function were revealed. As we previously reported for chronically HIV-infected individuals, we found that IgGs that associate with MUC16 are also increased during chronic SIV infection. Purification and characterization of the MUC16-eluted IgG subpopulation in chronically infected rhesus macaques revealed that these antibodies have a distinct glycosylation profile from the overall plasma antibody population containing fucosylated bisecting glycans (Fig. 1E), which has an enriched MUC16 association (Fig. 1D). Beyond increased MUC16 binding, decreased Fc$\gamma$R binding, and a lack of ADCC function (Fig. 1D and Fig. 2 and 3), these MUC16-associated IgGs are enriched for certain SIV antigen specificities for whole antigen and linear epitopes. Together, these differences suggest that during specific humoral responses, the immune system has the potential to direct certain antigen specificities to be targeted to accumulate within the columnar epithelial glycocalyx, where MUC16 is expressed, in the upper FRT, lungs, and potentially even the surface of the eye (5, 11, 42). This observation is consistent with MUC16 association being a new effector function for IgGs. Although the results presented here are consistent with an antibody enrichment of mucosal barrier function, further study is required to determine if this localization within the glycocalyx barrier leads to trapping of the pathogen before it can reach underlying cells *in vivo*.

Consistent with the potential for such pathogen trapping, we previously reported that MUC16 could capture HIV through antibody-specific interactions in an *in vitro* assay (10). Here, we gain further mechanistic insights into this new potential effector function by showing that these MUC16-eluted antibodies have an alternative glycosylation pattern. As expected, this population of MUC16-eluted antibodies, enriched for fucosylated bisecting glycoforms, had decreased binding to Fc$\gamma$R, which prefers afucosylated bisecting glycoforms. Instead, the MUC16-enriched fucosylated bisecting glycoforms showed increased interactions with MUC16 and a loss of function in an ADCC assay relative to plasma antibody populations. Importantly, this pattern of enrichment was seen in all animals evaluated. Unexpectedly, the MUC16-enriched fucosylated bisecting glycoform antibody population was also enriched for certain specific native antigen populations in gp41. Likewise, there was an increased interaction with linear peptides encoding gp120-V2, gp120-V3, and the C-gp41 immunodominant domain (C-gp41-ID) (aa 618 to 632). There was also a concomitant decrease in the binding specificity for other linear peptides, including V3, C5, and the gp41-ID (aa 600 to 626). The inability of these antibodies to carry out ADCC is most likely due to the alteration in the glycosylation profile as revealed in the Fc$\gamma$R binding studies. Inefficient Fc$\gamma$R binding, which is necessary for efficient ADCC activity, would lead to decreased ADCC activity in this type of tissue culture assay system.

We propose that the antigen specificity of the binding antibodies reflects the local immune environment present at the site of infection. For example, it has been reported in many studies that a nonneutralizing antibody response to gp41 is typically seen first during HIV infection in humans (43). This is believed to be a consequence of antigen mimicry, where the virus stimulates previous responses to antigens of commensal bacteria in the gut (44–46). Therefore, some of these early antibodies generated to gp41 and expanding and optimizing previous commensal bacterial responses would be targeted to effector functions associated with mucosal barriers. It remains to be determined if similar antigen-specific responses are associated with the fucosylated bisecting glycoforms that we previously observed to be enriched for MUC16 association in humans after HIV infection (10). Given the results from this study, one could

speculate that a subpopulation of these gp41-specific antibodies is preferentially deployed to the MUC16-containing glycocalyx of mucosal sites to fortify the mucosal barrier against future virus exposure utilizing this novel effector function of mucin binding leading to immune exclusion through HIV tethering (43, 47–49). Fortifying the endocervical epithelium could be an important deterrent to transmission, especially since multiple models have shown that this site is the major portal of transmission (50–52). Therefore, taken together, data from these studies are consistent with a novel effector function of fortifying glycocalyx barrier function by adding a layer of pathogen-specific antibodies.

In this study, we extend our discovery of Fc receptors in MUC16 to the nonhuman primate model. A viable primate model will be necessary for the future evaluation of the potential role that this novel effector function might play in vaccine efficacy. Like in humans, we observe an increase in the concentration of plasma antibodies with the ability to interact with the MUC16 Fc receptors as the immune environment transitions to an inflammatory phenotype during chronic infection. This effector function, the tethering of antibodies to MUC16, would impart antigen binding specificities to the protective glycocalyx layer. Such tethering could function to trap pathogens, such as HIV, in the glycocalyx and neutralize the virus through a mechanism of immune exclusion.

Furthermore, the findings from this study suggest that the immune response has the potential to direct antibodies enriched for certain antigenic specificities to interact with MUC16 and enrich the relatively weak protective function of the glycocalyx. Because of the apparent glycoform specificity of the MUC16-IgG interaction, it is theoretically possible to optimize vaccine responses with certain adjuvants or vaccination sites to increase MUC16 tethering (20). Interestingly, this ability of MUC16 to tether antibodies through Fc-specific interactions could also be a function of other cell-associated mucins, such as MUC1 in the FRT and MUC13 in the gut (53, 54).

Defining the optimal determinants of IgG-MUC16 interactions could provide another potential correlate of protection during the evaluation of human and macaque vaccine trials. The study of additional cell-associated and secreted gel-forming mucins could identify additional undefined desirable effector function determinants, which could be optimized during vaccine development. By modifying adjuvant selection, delivery systems, and vaccination regimens, it should be possible to optimize antibody-mucin interactions of current inefficient vaccines and promote virion trapping at the mucosal defense line.

## MATERIALS AND METHODS

**Macaques.** Indian rhesus macaques were inoculated with SIVmac251 via vaginal challenge (rhesus macaques N998, CF35, BV74, R908, DI28, DL31, and DB53), rectal challenge (DE09), or penile inoculation (IT14, HA55, HC21, HC22, FF18, GH26, and BE94). Plasma was isolated ~150 days after infection. In addition, for a subset of animals (IT14, HA55, HC21, HC22, FF18, GH26, and BE94), preinfection plasma draws were conducted to serve as negative controls.

**Ethics statement.** All macaques (*Macaca mulatta*) were housed at the Tulane National Primate Research Center (TNPRC) in accordance with Association for Assessment and Accreditation of Laboratory Animal Care International standards. All primate studies were reviewed and approved by the Tulane University Institutional Animal Care and Use Committee under protocol number P0240. Rhesus macaques were provided *ad libitum* with monkey chow (Lab Fiber Plus primate diet-DT; PMI Nutrition International, St. Louis, MO) and supplemented with fruits, vitamins, and Noyes' treats (Research Diets, New Brunswick, NJ). All clinical procedures were carried out under the direction of a laboratory animal veterinarian and performed under anesthesia using ketamine, often in combination with tiletamine (Telazol), with all efforts made to minimize stress, improve housing conditions, and provide enrichment opportunities (e.g., objects to manipulate in the cage, varied food supplements, foraging and task-oriented feeding methods, and interaction with caregivers and research staff).

**Mass spectrometry-based glycan analysis.** Gel-excised IgG heavy chains (IgG purified from rhesus macaques HC21, GH26, and DL31) were digested with LysC in 100 mM Tris-HCl buffer (pH 8.25). Peptides were extracted by dehydration with a water-acetonitrile-formic acid solution (40:50:5) followed by a water-acetonitrile-formic acid solution (15:80:5), lyophilized, and resuspended in 0.5% formic acid. Liquid chromatography-mass spectrometry (LC-MS) was carried out using a Q-Exactive Orbitrap (Thermo Scientific) or a Velos Orbitrap Elite (Thermo Scientific) mass spectrometer. The relative amounts of each N-glycan-modified species were determined by summing the total intensity from all of the observed charge states in the mass range of $m/z$ 500 to 2,000 with an error of 10 ppm measured using Xtract

(Thermo Scientific). Parallel titrations of input IgG were analyzed to establish that the observed amounts of each species are in the linear range of detection. The total intensity from all 16 N-glycans profiled was used to normalize the total intensity across each sample in order to compare the relative amounts of each N-glycan species. All samples were run in technical triplicates. To measure the percent increase for particular glycoforms, the normalized intensity for the MUC16-eluted IgG was divided by the normalized intensity for the input IgG.

**Immunofluorescence.** Sectioned frozen endocervical macaque tissues were fixed in 3.7% formaldehyde in PIPES [piperazine-*N*,*N*′-bis(2-ethanesulfonic acid)] buffer and blocked with normal donkey serum prior to staining. For adherens junction identification, anti-E-cadherin-488 (clone 36; BD Biosciences) was used. To identify MUC16 expression, tissues were stained with anti-muc16 (clone oct125; Abcam). A donkey anti-mouse secondary antibody, labeled with Cy5 (Jackson ImmunoResearch), was also utilized. Antibody specificity was confirmed by negative results with the respective isotype and secondary control antibodies. Hoechst (Invitrogen) was used for staining of nuclear material. After staining, mounting medium (DakoCytomation) and coverslips were applied and sealed with clear nail polish.

**Imaging and image analysis.** Images were obtained by deconvolution microscopy on a DeltaVision RT system collected on a digital camera (CoolSNAP HQ; Photometrics) using a 100× oil objective.

**MUC16 capture assay.** IgG was isolated from rhesus macaque plasma using protein $G^+$-agarose beads (Thermo Fisher) according to the manufacturer's instructions. Five micrograms of a recombinant human CA125 fragment of MUC16 (aa 13360 to Gln14347; R&D Systems) was covalently bound to 30 $\mu$l of tosyl-activated M-280 magnetic beads (Life Technologies) overnight at 37°C with rotation end over end in 300 $\mu$l 3 M ammonium sulfate–0.1 M sodium phosphate buffer. MUC16-bound beads were next aspirated, and 50 $\mu$g of purified IgG was added in 0.1 M sodium phosphate buffer with rotation end over end at room temperature (RT) for 4 h. This was scaled up to 10 reactions for a total of 50 $\mu$g MUC16 and 500 $\mu$g of IgG per rhesus macaque. Beads were washed 3 times with PBS with 1% Tween 20. MUC16-IgG beads from these 10 reaction mixtures were next pooled, and Abs were eluted in 100 $\mu$l 6 M guanidine HCl, followed by buffer exchange into PBS using 40,000-molecular-weight-cutoff (MWCO), 0.5-ml Zeba spin desalting columns (Thermo Scientific). This was repeated for IgG from each animal. As a control, input antibodies were incubated with 6 M guanidine HCl for 10 min and buffer exchanged into PBS. The percent yield of MUC16-eluted IgG was calculated by dividing the amount of MUC16-eluted antibody by the total IgG incubated with MUC16 beads. To ensure that IgG was efficiently eluted and was not degraded during the purification process, 10 $\mu$l of the eluate was compared to 10 $\mu$g of the input IgG by SDS-polyacrylamide gel electrophoresis followed by Coomassie staining with SimplyBlue safe stain (Thermo Fisher Scientific).

**MUC16 binding ELISA.** A recombinant human CA125 fragment of MUC16 (aa 13360 to Gln14347; R&D Systems) was immobilized onto Ni-nitrilotriacetic acid (NTA) HISSorb plates (catalog number 35061; Qiagen) at 1 $\mu$g/ml overnight at 4°C. Plates were washed with PBS containing 0.05% Tween 20, 3 times between each step. Plates were blocked with bovine serum albumin (BSA) (5% in PBS) for 2 h. Purified rhesus macaque IgG samples were added in triplicate at 0.1 mg/ml and incubated for 2 h with rocking at RT. Anti-human IgG horseradish peroxidase (HRP) secondary antibody (catalog number 214-1002; Kirkegaard & Perry Laboratories, Inc. [KPL]) was added at 100 $\mu$l per well at 2 $\mu$g/ml for 1 h at RT, covered. The OPD (*O*-phenylenediamine) substrate (catalog number P5412; Sigma) diluted in phosphate citrate–$H_2O_2$ buffer was added at 50 $\mu$l/well. Reactions were stopped with 2.5 N $H_2SO_4$ at 50 $\mu$l/well. Plates were then read at an optical density at 492 nm ($OD_{492}$) on a FLUOstar Optima plate reader (BMG Labtech). Binding was tested for IgG purified from plasma before and after infection in Fig. 1B (rhesus macaques IT14, HA55, HC21, HC22, FF18, GH26, and BE94). In addition, MUC16-eluted IgG and control input IgG were assessed to show efficient enrichment in MUC16 binding IgG in Fig. 1D (rhesus macaques IT14, HA55, R908, CF35, and BE94).

**Enzyme-linked immunosorbent assay of FcγR binding.** Rhesus macaque FcγR binding of purified rhesus macaque IgG was quantified by an enzyme-linked immunosorbent assay (ELISA). Nickel plates (catalog number 15442; Pierce) were coated overnight at RT with recombinant macaque His-tagged FcγR (55) diluted to 0.2 $\mu$g/ml in PBS. The following day, the plates were blocked for 1 h at RT with blocking solution (25 nM Tris-buffered saline [TBS], 0.5% BSA, 0.05% Tween 20) and subsequently washed once with washing buffer (0.05% Tween 20 in PBS). To test the ability of MUC16-eluted fractions of macaque IgG (isolated from $SIV^+$ animals R908, IT24, and HA55) to bind the low-affinity FcγRs, the IgGs were titrated in a 4-fold dilution series from 20 $\mu$g/ml to 0.062 ng/ml and incubated for 2 h at RT on the FcγR-coated plate. After washing twice, bound antibodies were detected using HRP-conjugated goat $Fab_2$ anti-human IgG(H+L) (catalog number 214-1006; KPL) added at a dilution of 1:1,500 for 1 h at RT. After washing, 100 $\mu$l of the 3,3′,5,5′-tetramethylbenzidine (TMB) substrate (Southern Biotech) was added to each well, and reactions were stopped by adding 50 $\mu$l/well 2 N $H_2SO_4$. The absorbance was measured at 450 nm, with optical correction at 540 nm or 570 nm, using a SpectraMax M2 instrument (Molecular Device). Data are displayed as the median values for the 3 monkeys in the antibody titration graphs, with the area under the curve (AUC) for each individual monkey at the right.

**Rapid fluorometric antibody-mediated cellular cytotoxicity assay.** We characterized the antibody-mediated cellular cytotoxicity (ADCC) activity profile of antibodies isolated from 4 SIV-infected (IT14, HA55, GH26, and R908) and 3 uninfected (IT14, GH26, and BE94) animals. Specifically, for each animal, we tested the input IgG, GuHCl-treated input IgG, and MUC16-eluted IgG. We used an optimized rapid fluorometric ADCC (RFADCC) assay to measure ADCC, as reported previously (40). Briefly, $1 \times 10^6$ EGFP-CEM-NKr-CCR5-snap cells, sensitized with recombinant SIV CM239 AT-2 inactivated virus (38 $\mu$l of virus with a p27 concentration of 362 ng/$\mu$l [~13.75 $\mu$g]) (56) by spinoculation (2 h at 2,000 rpm at 12°C),

were used as targets, and human PBMCs were utilized as effector cells. This concentration of virus was chosen based on results showing that CM239 virions have an average of 2,000 molecules of p27 (57). Human PBMCs were used as they have lower background levels than monkey PBMCs in this assay (58). The antibody activity was analyzed with 3-fold serial dilutions starting from a concentration of 10 $\mu$g/ml. At the end of the reaction with IgG (2 h), the fixed samples were acquired (approximately 35,000 events/sample) on a BD Fortessa special-order instrument (BD Biosciences) and analyzed using FlowJo software (TreeStar, Ashland, OR). ADCC activity (percent cytotoxicity) is defined as the percentage of EGFP-CEM-NKr-CCR5-snap target cells that lose EGFP staining but retain the CCR5-snap tag dye (gate P3) compared to the total number of target cells (gate P2). We used an SIV-specific rhesus macaque IgG, 311.H (gp120 V3 loop) (59, 60), as a positive control and 6.10B (gp120 CD4bS and CCR5bS) (61) and Synagis (anti-respiratory syncytial virus; MedImmune) as negative controls for ADCC. Each IgG sample from each individual monkey was tested in triplicate in two independent experiments. The means of the triplicates for each monkey were calculated within each experiment, and a final mean from each of these triplicates was then calculated over the 2 experiments. Data are displayed as the median values for each group of monkeys in the antibody titration graph and areas under the curve for GuHCl SIV$^+$ versus MUC16-eluted SIV$^+$ individual monkeys.

**SIV binding antibody multiplex assay.** The SIV antigen binding specificities of the different eluted IgG fractions, MUC16-binding IgG, input IgG, and GuHCl-treated input IgG, from macaques were determined by a custom SIV binding antibody multiplex assay (BAMA) as previously described (41). Briefly, a total of $5 \times 10^6$ carboxylated fluorescent beads (Luminex Corp., Austin, TX) were covalently coupled to 25 $\mu$g of one of the purified SIV antigens (recombinant SIVmac239 gp120 [Immune Technology, New York, NY], SIV p55 [Protein Sciences, Meriden, CT], SIV gp140 [of strain SIVMac32H {62}, kindly provided by Bing Chen, Harvard University, Boston, MA], gp130 SIVmac251 [ImmunoDiagnostics, Gaithersburg, MD], recombinant SIV gp41 [ImmunoDiagnostics, Gaithersburg, MD], SIV p27 [ImmunoDiagnostics, Gaithersburg, MD], and SIVsmE660 gp140 [Immune Technology, New York, NY]) and incubated with the eluted IgG fractions for 30 min. SIV-specific IgG was detected with anti-monkey IgG conjugated to biotin, at 4 $\mu$g/ml, followed by washing and incubation with streptavidin-phycoerythrin (PE) (BD Pharmingen). Beads were then washed and acquired on a Bio-Plex instrument (Bio-Rad, Hercules, CA), and the readout was in mean fluorescence intensities (MFIs). Each sample was titrated (run at multiple dilutions [1:5, 1:20, 1:80, 1:320, 1:1,280, and 1:5,120]). The first dilution at which the blank and background-subtracted MFI was within the linear range of the assay was chosen for reporting. For samples that were above the linear range of the assay at all dilutions tested, the MFI was set to the upper limit for analysis purposes. IgG BAMA specific activity was determined to normalize the antigen-specific binding magnitude with the IgG concentration in each sample. Specific activity was calculated as the ratio of (blank and background-subtracted MFI $\times$ dilution)/total IgG (micrograms per milliliter), which was measured by a macaque IgG ELISA. All assays were run under good clinical laboratory practice (GCLP)-compliant conditions, including tracking of positive controls by using Levy-Jennings charts. The rhesus macaques assessed with the BAMA were HC21, GH26, IT14, HA55, HC22, FF18, BE94, N998, R908, BV74, CF35, DE09, DI28, and DL31.

**Linear epitope mapping for SIV Env.** Linear epitope mapping of the MUC16 binding IgG and GuHCl-treated input IgG from rhesus macaques against SIV Env was performed as previously described, with minor modifications (41, 63). Microarray slides in a quad-chamber format were provided by JPT Peptide Technologies GmbH (Germany) by printing a library designed by B. Korber, Los Alamos National Laboratory, onto epoxy glass slides (PolyAn GmbH, Germany). The library contains overlapping peptides (15-mers overlapping by 12 aa) covering full-length Env sequences for SIVmac239 and SIVsmE660. Three identical subarrays, each containing the entire peptide library, were printed in each hybridization area. All array slides were blocked with PBS containing 1% powdered milk, 5% normal goat serum, and 0.05% Tween for 1 h, followed by a 2-h incubation with each purified IgG fraction diluted in blocking buffer to 3.9 $\mu$g/ml of IgG and a subsequent 45-min incubation with goat anti-human IgG conjugated with Alexa Fluor 647 (AF647; Jackson ImmunoResearch, PA). Array slides were scanned at a wavelength of 635 nm with an InnoScan 710 AL scanner (Innopsys, Carbonne, France) using XDR (extended dynamic range) mode. Scan images were analyzed using Mapix 8.0 software to obtain fluorescence intensity values for all peptides. Binding magnitudes for epitopes that were targeted by the samples were summarized. The magnitude of binding for each identified epitope was defined as the highest binding by a single peptide within the epitope region. Linear peptide binding was assessed for rhesus macaques HC21, GH26, BE94, N998, BV74, DE09, DI28, and DL31.

**Statistical analysis.** Statistical analysis for comparisons of responses between matched samples was performed using a sign test. The results from comparisons between matched GuHCl- and MUC16-eluted samples (Fig. 4 and 5) were corrected for multiple testing using the Benjamini-Hochberg false discovery rate (FDR) method (64). The raw *P* values are the *P* values from the individual sign tests, and the FDR *P* values are the Benjamini-Hochberg (64)-corrected *P* values. The alpha level was set to 0.05. *P* values of $<0.05$ were considered statistically significant, indicating that the median difference in the responses between the matched samples is not equal to zero. The AUC was calculated using the trapezoidal method. The percent reduction of the AUC was calculated by subtracting the median AUC for MUC16-eluted IgG from the median AUC for GuHCl-treated input IgG and dividing this value by the median AUC for GuHCl-treated IgG. The analysis was performed using SAS proprietary software 9.4 (TS1M2) (2002 to 2012; SAS Institute, Inc., Cary, NC, USA). Graphs were generated in R 0.99.491 and GraphPad Prism 7.

## ACKNOWLEDGMENTS

This work was supported by Bill and Melinda Gates Foundation (BMGF) grant OPP1031734 (T.J.H.), National Institutes of Health (NIH) NIAID grants R01-AI125171 (T.J.H.), K01 OD024882-01 (J.R.S.), PO1-A1120756 (G.K.L., X.S., and G.D.T.), 5P30AI06518 (X.S. and G.D.T.), and P41 GM108569 (N.L.K). The Bill and Melinda Gates Foundation CAVD Exchange OPP1084285 between the Hope lab and Lewis lab was instrumental in setting up key experiments carried out in the manuscript.

We thank Joern E. Schmitz and Sarah Cocklin (Harvard Medical School) for the kind gifts of the rhesus macaque FcγRs. We thank Judith T. Lucas, Sam McMillan, Ryan Duffy, David Beaumont, and Vicki Ashley for expert technical assistance with the antigen specificity assays. We give special thanks to Arangassery Rosemary Bastian, Flora Engelmann, and Patrick Madden for helpful editing of the manuscript.

J.R.S. isolated MUC16-associated IgG and carried out MUC16 ELISAs. J.R.S. and A.D.S. carried out glycoform mass spectrometry, and N.L.K. advised. J.R.S. and C.O. carried out the FcγR ELISAs and RFADCC assays, and G.K.L. advised. J.R.S. and A.M.C. carried out microscopy. X.S. and T.N. carried out the whole-antigen and linear antigen peptide binding assays, and G.D.T. advised. R.S.V. carried out the SIV infections and rhesus macaque sample collection. S.S. assisted with statistical analysis. J.R.S. wrote the manuscript, and T.J.H. assisted with experimental design and manuscript preparation.

There are no competing interests to disclose.

## REFERENCES

1. Haynes BF, Gilbert PB, McElrath MJ, Zolla-Pazner S, Tomaras GD, Alam SM, Evans DT, Montefiori DC, Karnasuta C, Sutthent R, Liao HX, DeVico AL, Lewis GK, Williams C, Pinter A, Fong Y, Janes H, DeCamp A, Huang Y, Rao M, Billings E, Karasavvas N, Robb ML, Ngauy V, de Souza MS, Paris R, Ferrari G, Bailer RT, Soderberg KA, Andrews C, Berman PW, Frahm N, De Rosa SC, Alpert MD, Yates NL, Shen X, Koup RA, Pitisuttithum P, Kaewkungwal J, Nitayaphan S, Rerks-Ngarm S, Michael NL, Kim JH. 2012. Immune-correlates analysis of an HIV-1 vaccine efficacy trial. N Engl J Med 366:1275–1286. https://doi.org/10.1056/NEJMoa1113425.
2. Barouch DH, Liu J, Li H, Maxfield LF, Abbink P, Lynch DM, Iampietro MJ, SanMiguel A, Seaman MS, Ferrari G, Forthal DN, Ourmanov I, Hirsch VM, Carville A, Mansfield KG, Stablein D, Pau MG, Schuitemaker H, Sadoff JC, Billings EA, Rao M, Robb ML, Kim JH, Marovich MA, Goudsmit J, Michael NL. 2012. Vaccine protection against acquisition of neutralization-resistant SIV challenges in rhesus monkeys. Nature 482:89–93. https://doi.org/10.1038/nature10766.
3. Barouch DH, Stephenson KE, Borducchi EN, Smith K, Stanley K, McNally AG, Liu J, Abbink P, Maxfield LF, Seaman MS, Dugast AS, Alter G, Ferguson M, Li W, Earl PL, Moss B, Giorgi EE, Szinger JJ, Eller LA, Billings EA, Rao M, Tovanabutra S, Sanders-Buell E, Weijtens M, Pau MG, Schuitemaker H, Robb ML, Kim JH, Korber BT, Michael NL. 2013. Protective efficacy of a global HIV-1 mosaic vaccine against heterologous SHIV challenges in rhesus monkeys. Cell 155:531–539. https://doi.org/10.1016/j.cell.2013.09.061.
4. Hope TJ. 2011. Moving ahead an HIV vaccine: to neutralize or not, a key HIV vaccine question. Nat Med 17:1195–1197. https://doi.org/10.1038/nm.2528.
5. Andersch-Bjorkman Y, Thomsson KA, Holmen Larsson JM, Ekerhovd E, Hansson GC. 2007. Large scale identification of proteins, mucins, and their O-glycosylation in the endocervical mucus during the menstrual cycle. Mol Cell Proteomics 6:708–716. https://doi.org/10.1074/mcp.M600439-MCP200.
6. Gipson IK, Blalock T, Tisdale A, Spurr-Michaud S, Allcorn S, Stavreus-Evers A, Gemzell K. 2008. MUC16 is lost from the uterodome (pinopode) surface of the receptive human endometrium: in vitro evidence that MUC16 is a barrier to trophoblast adherence. Biol Reprod 78:134–142. https://doi.org/10.1095/biolreprod.106.058347.
7. Fahrbach KM, Malykhina O, Stieh DJ, Hope TJ. 2013. Differential binding of IgG and IgA to mucus of the female reproductive tract. PLoS One 8:e76176. https://doi.org/10.1371/journal.pone.0076176.
8. Wang YY, Kannan A, Nunn KL, Murphy MA, Subramani DB, Moench T, Cone R, Lai SK. 2014. IgG in cervicovaginal mucus traps HSV and prevents vaginal herpes infections. Mucosal Immunol 7:1036–1044. https://doi.org/10.1038/mi.2013.120.
9. Forthal D, Hope TJ, Alter G. 2013. New paradigms for functional HIV-specific nonneutralizing antibodies. Curr Opin HIV AIDS 8:393–401. https://doi.org/10.1097/COH.0b013e328363d486.
10. Gunn BM, Schneider JR, Shansab M, Bastian AR, Fahrbach KM, Smith AD, IV, Mahan AE, Karim MM, Licht AF, Zvonar I, Tedesco J, Anderson MR, Chapel A, Suscovich TJ, Malaspina DC, Streeck H, Walker BD, Kim A, Lauer G, Altfeld M, Pillai S, Szleifer I, Kelleher NL, Kiser PF, Hope TJ, Alter G. 2016. Enhanced binding of antibodies generated during chronic HIV infection to mucus component MUC16. Mucosal Immunol 9:1549–1558. https://doi.org/10.1038/mi.2016.8.
11. Kanwal M, Ding XJ, Song X, Zhou GB, Cao Y. 2018. MUC16 overexpression induced by gene mutations promotes lung cancer cell growth and invasion. Oncotarget 9:12226–12239. https://doi.org/10.18632/oncotarget.24203.
12. Stieh DJ, Maric D, Kelley ZL, Anderson MR, Hattaway HZ, Beilfuss BA, Rothwangl KB, Veazey RS, Hope TJ. 2014. Vaginal challenge with an SIV-based dual reporter system reveals that infection can occur throughout the upper and lower female reproductive tract. PLoS Pathog 10:e1004440. https://doi.org/10.1371/journal.ppat.1004440.
13. Stieh DJ, Matias E, Xu H, Fought AJ, Blanchard JL, Marx PA, Veazey RS, Hope TJ. 2016. Th17 cells are preferentially infected very early after vaginal transmission of SIV in macaques. Cell Host Microbe 19:529–540. https://doi.org/10.1016/j.chom.2016.03.005.
14. Stokes CR, Soothill JF, Turner MW. 1975. Immune exclusion is a function of IgA. Nature 255:745–746. https://doi.org/10.1038/255745a0.
15. Ruprecht RM, Lakhashe SK. 2017. Antibody-mediated immune exclusion of HIV. Curr Opin HIV AIDS 12:222–228. https://doi.org/10.1097/COH.0000000000000369.
16. Watkins JD, Sholukh AM, Mukhtar MM, Siddappa NB, Lakhashe SK, Kim M, Reinherz EL, Gupta S, Forthal DN, Sattentau QJ, Villinger F, Corti D, Ruprecht RM, CAVD Project Group. 2013. Anti-HIV IgA isotypes: differential virion capture and inhibition of transcytosis are linked to prevention of mucosal R5 SHIV transmission. AIDS 27:F13–F20. https://doi.org/10.1097/QAD.0b013e328360eac6.
17. Sholukh AM, Watkins JD, Vyas HK, Gupta S, Lakhashe SK, Thorat S, Zhou M, Hemashettar G, Bachler BC, Forthal DN, Villinger F, Sattentau QJ, Weiss RA, Agatic G, Corti D, Lanzavecchia A, Heeney JL, Ruprecht RM. 2015. Defense-in-depth by mucosally administered anti-HIV dimeric IgA2 and systemic IgG1 mAbs: complete protection of rhesus monkeys from mucosal SHIV challenge. Vaccine 33:2086–2095. https://doi.org/10.1016/j.vaccine.2015.02.020.

18. Gong S, Tomusange K, Kulkarni V, Adeniji OS, Lakhashe SK, Hariraju D, Strickland A, Plake E, Frost PA, Ratcliffe SJ, Wang L, Lafer EM, Ruprecht RM. 2018. Anti-HIV IgM protects against mucosal SHIV transmission. AIDS 32:F5–F13. https://doi.org/10.1097/QAD.0000000000001857.
19. Moore JS, Wu X, Kulhavy R, Tomana M, Novak J, Moldoveanu Z, Brown R, Goepfert PA, Mestecky J. 2005. Increased levels of galactose-deficient IgG in sera of HIV-1-infected individuals. AIDS 19:381–389. https://doi.org/10.1097/01.aids.0000161767.21405.68.
20. Alter G, Ottenhoff THM, Joosten SA. 2018. Antibody glycosylation in inflammation, disease and vaccination. Semin Immunol 39:102–110. https://doi.org/10.1016/j.smim.2018.05.003.
21. Ward E, Mittereder N, Kuta E, Sims GP, Bowen MA, Dall'Acqua W, Tedder T, Kiener P, Coyle AJ, Wu H, Jallal B, Herbst R. 2011. A glycoengineered anti-CD19 antibody with potent antibody-dependent cellular cytotoxicity activity in vitro and lymphoma growth inhibition in vivo. Br J Haematol 155:426–437. https://doi.org/10.1111/j.1365-2141.2011.08857.x.
22. Ferrara C, Grau S, Jager C, Sondermann P, Brunker P, Waldhauer I, Hennig M, Ruf A, Rufer AC, Stihle M, Umana P, Benz J. 2011. Unique carbohydrate-carbohydrate interactions are required for high affinity binding between FcgammaRIII and antibodies lacking core fucose. Proc Natl Acad Sci U S A 108:12669–12674. https://doi.org/10.1073/pnas.1108455108.
23. Shields RL, Lai J, Keck R, O'Connell LY, Hong K, Meng YG, Weikert SHA, Presta LG. 2002. Lack of fucose on human IgG1 N-linked oligosaccharide improves binding to human Fcgamma RIII and antibody-dependent cellular toxicity. J Biol Chem 277:26733–26740. https://doi.org/10.1074/jbc.M202069200.
24. Davies J, Jiang L, Pan LZ, LaBarre MJ, Anderson D, Reff M. 2001. Expression of GnTIII in a recombinant anti-CD20 CHO production cell line: expression of antibodies with altered glycoforms leads to an increase in ADCC through higher affinity for FC gamma RIII. Biotechnol Bioeng 74:288–294. https://doi.org/10.1002/bit.1119.
25. Ackerman ME, Crispin M, Yu X, Baruah K, Boesch AW, Harvey DJ, Dugast AS, Heizen EL, Ercan A, Choi I, Streeck H, Nigrovic PA, Bailey-Kellogg C, Scanlan C, Alter G. 2013. Natural variation in Fc glycosylation of HIV-specific antibodies impacts antiviral activity. J Clin Invest 123:2183–2192. https://doi.org/10.1172/JCI65708.
26. DiLillo DJ, Tan GS, Palese P, Ravetch JV. 2014. Broadly neutralizing hemagglutinin stalk-specific antibodies require FcgammaR interactions for protection against influenza virus in vivo. Nat Med 20:143–151. https://doi.org/10.1038/nm.3443.
27. Huber VC, Lynch JM, Bucher DJ, Le J, Metzger DW. 2001. Fc receptor-mediated phagocytosis makes a significant contribution to clearance of influenza virus infections. J Immunol 166:7381–7388. https://doi.org/10.4049/jimmunol.166.12.7381.
28. Bournazos S, Chow SK, Abboud N, Casadevall A, Ravetch JV. 2014. Human IgG Fc domain engineering enhances antitoxin neutralizing antibody activity. J Clin Invest 124:725–729. https://doi.org/10.1172/JCI72676.
29. Bournazos S, Klein F, Pietzsch J, Seaman MS, Nussenzweig MC, Ravetch JV. 2014. Broadly neutralizing anti-HIV-1 antibodies require Fc effector functions for in vivo activity. Cell 158:1243–1253. https://doi.org/10.1016/j.cell.2014.08.023.
30. Bruel T, Guivel-Benhassine F, Amraoui S, Malbec M, Richard L, Bourdic K, Donahue DA, Lorin V, Casartelli N, Noel N, Lambotte O, Mouquet H, Schwartz O. 2016. Elimination of HIV-1-infected cells by broadly neutralizing antibodies. Nat Commun 7:10844. https://doi.org/10.1038/ncomms10844.
31. Hessell AJ, Hangartner L, Hunter M, Havenith CE, Beurskens FJ, Bakker JM, Lanigan CM, Landucci G, Forthal DN, Parren PW, Marx PA, Burton DR. 2007. Fc receptor but not complement binding is important in antibody protection against HIV. Nature 449:101–104. https://doi.org/10.1038/nature06106.
32. Pauthner MG, Nkolola JP, Havenar-Daughton C, Murrell B, Reiss SM, Bastidas R, Prevost J, Nedellec R, von Bredow B, Abbink P, Cottrell CA, Kulp DW, Tokatlian T, Nogal B, Bianchi M, Li H, Lee JH, Butera ST, Evans DT, Hangartner L, Finzi A, Wilson IA, Wyatt RT, Irvine DJ, Schief WR, Ward AB, Sanders RW, Crotty S, Shaw GM, Barouch DH, Burton DR. 2019. Vaccine-induced protection from homologous tier 2 SHIV challenge in nonhuman primates depends on serum-neutralizing antibody titers. Immunity 50:241–252. https://doi.org/10.1016/j.immuni.2018.11.011.
33. Parsons MS, Lee WS, Kristensen AB, Amarasena T, Khoury G, Wheatley AK, Reynaldi A, Wines BD, Hogarth PM, Davenport MP, Kent SJ. 2019. Fc-dependent functions are redundant to efficacy of anti-HIV antibody PGT121 in macaques. J Clin Invest 129:182–191. https://doi.org/10.1172/JCI122466.
34. Forthal D, Finzi A. 2019. Blocking HIV-1 replication: are Fc-Fcgamma receptor interactions required? J Clin Invest 129:53–54. https://doi.org/10.1172/JCI125264.
35. Mir KD, Gasper MA, Sundaravaradan V, Sodora DL. 2011. SIV infection in natural hosts: resolution of immune activation during the acute-to-chronic transition phase. Microbes Infect 13:14–24. https://doi.org/10.1016/j.micinf.2010.09.011.
36. Kaul M, Loos M. 1997. Dissection of C1q capability of interacting with IgG. Time-dependent formation of a tight and only partly reversible association. J Biol Chem 272:33234–33244. https://doi.org/10.1074/jbc.272.52.33234.
37. Huang Y, Gilbert PB, Montefiori DC, Self SG. 2009. Simultaneous evaluation of the magnitude and breadth of a left and right censored multivariate response, with application to HIV vaccine development. Stat Biopharm Res 1:81–91. https://doi.org/10.1198/sbr.2009.0008.
38. Yu X, Gilbert PB, Hioe CE, Zolla-Pazner S, Self SG. 2012. Statistical approaches to analyzing HIV-1 neutralizing antibody assay data. Stat Biopharm Res 4:1–13. https://doi.org/10.1080/19466315.2011.633860.
39. Chung AW, Crispin M, Pritchard L, Robinson H, Gorny MK, Yu X, Bailey-Kellogg C, Ackerman ME, Scanlan C, Zolla-Pazner S, Alter G. 2014. Identification of antibody glycosylation structures that predict monoclonal antibody Fc-effector function. AIDS 28:2523–2530. https://doi.org/10.1097/QAD.0000000000000444.
40. Orlandi C, Flinko R, Lewis GK. 2016. A new cell line for high throughput HIV-specific antibody-dependent cellular cytotoxicity (ADCC) and cell-to-cell virus transmission studies. J Immunol Methods 433:51–58. https://doi.org/10.1016/j.jim.2016.03.002.
41. Tomaras GD, Binley JM, Gray ES, Crooks ET, Osawa K, Moore PL, Tumba N, Tong T, Shen X, Yates NL, Decker J, Wibmer CK, Gao F, Alam SM, Easterbrook P, Abdool Karim S, Kamanga G, Crump JA, Cohen M, Shaw GM, Mascola JR, Haynes BF, Montefiori DC, Morris L. 2011. Polyclonal B cell responses to conserved neutralization epitopes in a subset of HIV-1-infected individuals. J Virol 85:11502–11519. https://doi.org/10.1128/JVI.05363-11.
42. Argueso P, Spurr-Michaud S, Russo CL, Tisdale A, Gipson IK. 2003. MUC16 mucin is expressed by the human ocular surface epithelia and carries the H185 carbohydrate epitope. Invest Ophthalmol Vis Sci 44:2487–2495. https://doi.org/10.1167/iovs.02-0862.
43. Tomaras GD, Yates NL, Liu P, Qin L, Fouda GG, Chavez LL, Decamp AC, Parks RJ, Ashley VC, Lucas JT, Cohen M, Eron J, Hicks CB, Liao HX, Self SG, Landucci G, Forthal DN, Weinhold KJ, Keele BF, Hahn BH, Greenberg ML, Morris L, Karim SS, Blattner WA, Montefiori DC, Shaw GM, Perelson AS, Haynes BF. 2008. Initial B-cell responses to transmitted human immunodeficiency virus type 1: virion-binding immunoglobulin M (IgM) and IgG antibodies followed by plasma anti-gp41 antibodies with ineffective control of initial viremia. J Virol 82:12449–12463. https://doi.org/10.1128/JVI.01708-08.
44. Trama AM, Moody MA, Alam SM, Jaeger FH, Lockwood B, Parks R, Lloyd KE, Stolarchuk C, Scearce R, Foulger A, Marshall DJ, Whitesides JF, Jeffries TL, Jr, Wiehe K, Morris L, Lambson B, Soderberg K, Hwang KK, Tomaras GD, Vandergrift N, Jackson KJL, Roskin KM, Boyd SD, Kepler TB, Liao HX, Haynes BF. 2014. HIV-1 envelope gp41 antibodies can originate from terminal ileum B cells that share cross-reactivity with commensal bacteria. Cell Host Microbe 16:215–226. https://doi.org/10.1016/j.chom.2014.07.003.
45. Liao HX, Chen X, Munshaw S, Zhang R, Marshall DJ, Vandergrift N, Whitesides JF, Lu X, Yu JS, Hwang KK, Gao F, Markowitz M, Heath SL, Bar KJ, Goepfert PA, Montefiori DC, Shaw GC, Alam SM, Margolis DM, Denny TN, Boyd SD, Marshal E, Egholm M, Simen BB, Hanczaruk B, Fire AZ, Voss G, Kelsoe G, Tomaras GD, Moody MA, Kepler TB, Haynes BF. 2011. Initial antibodies binding to HIV-1 gp41 in acutely infected subjects are polyreactive and highly mutated. J Exp Med 208:2237–2249. https://doi.org/10.1084/jem.20110363.
46. Williams WB, Liao HX, Moody MA, Kepler TB, Alam SM, Gao F, Wiehe K, Trama AM, Jones K, Zhang R, Song H, Marshall DJ, Whitesides JF, Sawatzki K, Hua A, Liu P, Tay MZ, Seaton KE, Shen X, Foulger A, Lloyd KE, Parks R, Pollara J, Ferrari G, Yu JS, Vandergrift N, Montefiori DC, Sobieszczyk ME, Hammer S, Karuna S, Gilbert P, Grove D, Grunenberg N, McElrath MJ, Mascola JR, Koup RA, Corey L, Nabel GJ, Morgan C, Churchyard G, Maenza J, Keefer M, Graham BS, Baden LR, Tomaras GD, Haynes BF. 2015. HIV-1 vaccines. Diversion of HIV-1 vaccine-induced immunity by gp41-

microbiota cross-reactive antibodies. Science 349:aab1253. https://doi.org/10.1126/science.aab1253.
47. Liu P, Overman RG, Yates NL, Alam SM, Vandergrift N, Chen Y, Graw F, Freel SA, Kappes JC, Ochsenbauer C, Montefiori DC, Gao F, Perelson AS, Cohen MS, Haynes BF, Tomaras GD. 2011. Dynamic antibody specificities and virion concentrations in circulating immune complexes in acute to chronic HIV-1 infection. J Virol 85:11196–11207. https://doi.org/10.1128/JVI.05601-11.
48. Liu P, Williams LD, Shen X, Bonsignori M, Vandergrift NA, Overman RG, Moody MA, Liao HX, Stieh DJ, McCotter KL, French AL, Hope TJ, Shattock R, Haynes BF, Tomaras GD. 2014. Capacity for infectious HIV-1 virion capture differs by envelope antibody specificity. J Virol 88:5165–5170. https://doi.org/10.1128/JVI.03765-13.
49. Vaidya NK, Ribeiro RM, Liu P, Haynes BF, Tomaras GD, Perelson AS. 2018. Correlation between anti-gp41 antibodies and virus infectivity decay during primary HIV-1 infection. Front Microbiol 9:1326. https://doi.org/10.3389/fmicb.2018.01326.
50. Deleage C, Immonen TT, Fennessey CM, Reynaldi A, Reid C, Newman L, Lipkey L, Schlub TE, Camus C, O'Brien S, Smedley J, Conway JM, Del Prete GQ, Davenport MP, Lifson JD, Estes JD, Keele BF. 2019. Defining early SIV replication and dissemination dynamics following vaginal transmission. Sci Adv 5:eaav7116. https://doi.org/10.1126/sciadv.aav7116.
51. Haase AT. 2010. Targeting early infection to prevent HIV-1 mucosal transmission. Nature 464:217–223. https://doi.org/10.1038/nature08757.
52. Li Q, Estes JD, Schlievert PM, Duan L, Brosnahan AJ, Southern PJ, Reilly CS, Peterson ML, Schultz-Darken N, Brunner KG, Nephew KR, Pambuccian S, Lifson JD, Carlis JV, Haase AT. 2009. Glycerol monolaurate prevents mucosal SIV transmission. Nature 458:1034–1038. https://doi.org/10.1038/nature07831.
53. Dharmaraj N, Chapela PJ, Morgado M, Hawkins SM, Lessey BA, Young SL, Carson DD. 2014. Expression of the transmembrane mucins, MUC1, MUC4 and MUC16, in normal endometrium and in endometriosis. Hum Reprod 29:1730–1738. https://doi.org/10.1093/humrep/deu146.
54. Sheng YH, Lourie R, Linden SK, Jeffery PL, Roche D, Tran TV, Png CW, Waterhouse N, Sutton P, Florin TH, McGuckin MA. 2011. The MUC13 cell-surface mucin protects against intestinal inflammation by inhibiting epithelial cell apoptosis. Gut 60:1661–1670. https://doi.org/10.1136/gut.2011.239194.
55. Chan YN, Boesch AW, Osei-Owusu NY, Emileh A, Crowley AR, Cocklin SL, Finstad SL, Linde CH, Howell RA, Zentner I, Cocklin S, Miles AR, Eckman JW, Alter G, Schmitz JE, Ackerman ME. 2016. IgG binding characteristics of rhesus macaque FcgammaR. J Immunol 197:2936–2947. https://doi.org/10.4049/jimmunol.1502252.
56. Guan Y, Pazgier M, Sajadi MM, Kamin-Lewis R, Al-Darmarki S, Flinko R, Lovo E, Wu X, Robinson JE, Seaman MS, Fouts TR, Gallo RC, DeVico AL, Lewis GK. 2013. Diverse specificity and effector function among human antibodies to HIV-1 envelope glycoprotein epitopes exposed by CD4 binding. Proc Natl Acad Sci U S A 110:E69–E78. https://doi.org/10.1073/pnas.1217609110.
57. Yuste E, Reeves JD, Doms RW, Desrosiers RC. 2004. Modulation of Env content in virions of simian immunodeficiency virus: correlation with cell surface expression and virion infectivity. J Virol 78:6775–6785. https://doi.org/10.1128/JVI.78.13.6775-6785.2004.
58. Gomez-Roman VR, Florese RH, Patterson LJ, Peng B, Venzon D, Aldrich K, Robert-Guroff M. 2006. A simplified method for the rapid fluorometric assessment of antibody-dependent cell-mediated cytotoxicity. J Immunol Methods 308:53–67. https://doi.org/10.1016/j.jim.2005.09.018.
59. Robinson JE, Cole KS, Elliott DH, Lam H, Amedee AM, Means R, Desrosiers RC, Clements J, Montelaro RC, Murphey-Corb M. 1998. Production and characterization of SIV envelope-specific rhesus monoclonal antibodies from a macaque asymptomatically infected with a live SIV vaccine. AIDS Res Hum Retroviruses 14:1253–1262. https://doi.org/10.1089/aid.1998.14.1253.
60. Cole KS, Alvarez M, Elliott DH, Lam H, Martin E, Chau T, Micken K, Rowles JL, Clements JE, Murphey-Corb M, Montelaro RC, Robinson JE. 2001. Characterization of neutralization epitopes of simian immunodeficiency virus (SIV) recognized by rhesus monoclonal antibodies derived from monkeys infected with an attenuated SIV strain. Virology 290:59–73. https://doi.org/10.1006/viro.2001.1144.
61. Swanstrom AE, Haggarty B, Jordan APO, Romano J, Leslie GJ, Aye PP, Marx PA, Lackner AA, Del Prete GQ, Robinson JE, Betts MR, Montefiori DC, LaBranche CC, Hoxie JA. 2016. Derivation and characterization of a CD4-independent, non-CD4-tropic simian immunodeficiency virus. J Virol 90:4966–4980. https://doi.org/10.1128/JVI.02851-15.
62. Chen B, Zhou G, Kim M, Chishti Y, Hussey RE, Ely B, Skehel JJ, Reinherz EL, Harrison SC, Wiley DC. 2000. Expression, purification, and characterization of gp160e, the soluble, trimeric ectodomain of the simian immunodeficiency virus envelope glycoprotein, gp160. J Biol Chem 275:34946–34953. https://doi.org/10.1074/jbc.M004905200.
63. Gottardo R, Bailer RT, Korber BT, Gnanakaran S, Phillips J, Shen X, Tomaras GD, Turk E, Imholte G, Eckler L, Wenschuh H, Zerweck J, Greene K, Gao H, Berman PW, Francis D, Sinangil F, Lee C, Nitayaphan S, Rerks-Ngarm S, Kaewkungwal J, Pitisuttithum P, Tartaglia J, Robb ML, Michael NL, Kim JH, Zolla-Pazner S, Haynes BF, Mascola JR, Self S, Gilbert P, Montefiori DC. 2013. Plasma IgG to linear epitopes in the V2 and V3 regions of HIV-1 gp120 correlate with a reduced risk of infection in the RV144 vaccine efficacy trial. PLoS One 8:e75665. https://doi.org/10.1371/journal.pone.0075665.
64. Benjamini Y, Hochberg Y. 1995. Controlling the false discovery rate: a practical and powerful approach to multiple testing. J R Stat Soc Series B Stat Methodol 57:289–300. https://doi.org/10.1111/j.2517-6161.1995.tb02031.x.